[409.05] HST/STIS High-Resolution Imaging of the HR 4796A Circumstellar Debris Ring

213th Meeting of the American Astronomical Society with HAD and HEAD
4-8 January 2009
Long Beach, CA
2009 International Year of Astronomy

* Contact: gschneider@as.arizona.edu

Glenn Schneider* (Univ. of Arizona), A. J. Weinberger (DTM, Carnegie Inst. of Washington), E. E. Becklin (UCLA), J. H. Debes (DTM, Carnegie Inst. of Washington), B. A. Smith (Univ. of Hawaii)

We present high spatial resolution coronagraphic imaging observations of the HR 4796A circumstellar debris dust ring that we obtained using the broad optical response of the Hubble Space Telescope Imaging Spectrograph. We use our visual wavelength observations to improve upon the earlier measured geometrical parameters of the ring-like disk originally determined from lower resolution HST/NICMOS observations. Two significant flux density asymmetries in the dust ring are noted: (1) preferential forward scattering by the disk grains and (2) an azimuthal surface brightness (SB) anisotropy about the morphological minor axis of the disk with corresponding differential ansal brightness. We find the debris ring offset from the location of the star by less than 1.4 AU, a shift insufficient to explain the differing brightnesses of the NE and SW ansae simply by the r^{-2} diminution of starlight. The STIS data also better quantify the radial confinement of the starlight-scattering circumstellar debris, to a characteristic region less than 14 AU in photometric half-width, with a significantly steeper inner truncation than outward falloff in radial SB. The inferred spatial distribution of the disk grains is consistent with the possibility of one or more unseen co-orbital planetary-mass perturbers. The colors of the disk grains are consistent with a collisionally evolved population of debris, possibly including ices reddened by radiation exposure to the central star.

INTRODUCTION

HR 4796A (spectral type A0V) is the primary member of a 72.8 ± 1.7 pc distant binary system with an estimated age of 8 ± 2 Myr. The existence of a dusty debris disk around HR 4796A was inferred by Jura (1991; ApJ 383 L79) from its thermal IR excess. He and collaborators later suggested grain growth into larger particles 40–200 AU from the star (Jura et al. 1995; ApJ 445 451). Koerner et al. (1998; ApJ 503, L83) and Jayawarhana et al. (1998; ApJ 503 L79) confirmed that prediction with 10—20 μm mid-IR observations indicative of dust emission 60—87 AU from the star. Schneider et al. (1999; ApJ 513 L127) imaged a < 18 AU wide starlight scattering debris ring, 76 AU from the star, with HST/NICMOS coronagraphy at 1.1 and 1.6 μm. The NICMOS images informed of an ansal brightness asymmetry, similarly seen in mid-IR observations by Telesco et al.(2000; ApJ 530 329) and modeled by Wyatt et al. (1999; ApJ 527 918). We now present higher (~ 70 mas) spatial resolution optical images of the HR 4796A debris ring that we obtained with the Space Telescope Imaging Spectrograph (STIS) in its coronagraphic imaging mode. From these data we examine in more detail the spatial distribution of the ring particles as inferred from spatially resolved imaging photometry along, and around, the ring. We confirm, and better quantify, the geometrical parameters defining the ring system and also measure two anisotropies in the photometric properties along the ring. These will be the highest angular resolution visible-light images of the HR 4796A debris ring for some time to come.

OBSERVATIONS & DATA

We obtained STIS broad-band (λ_{pivot} = 5752 Å, FWHM = 4330 Å) coronagraphic images (scale: 50.7 mas/pixel) of HR 4796A and HR 4748 (a nearby, similar spectral type, point spread function (PSF) reference star) with HST at two different spacecraft roll (field orientation) angles optimized to place the major axis of the disk between the HST diffraction spikes (*Fig 1*). After acquiring the targets, the stars were placed on the mid-line of the STIS image-plane mask where the tapered width of the occulting wedge is 0.63". Eighteen exposures of each star, at each field orientation, were obtained total integration times of 108 s and 76 s for HR 4796A and HR 4748 at each orientation, respectively. The raw data were reduced using the STSDAS calstis software and calibrated images for each target/orientation were median combined with cosmic-ray rejection. PSF subtraction analogously follows the method described (for NICMOS) by Schneider et al. (2001; AJ 121 525).

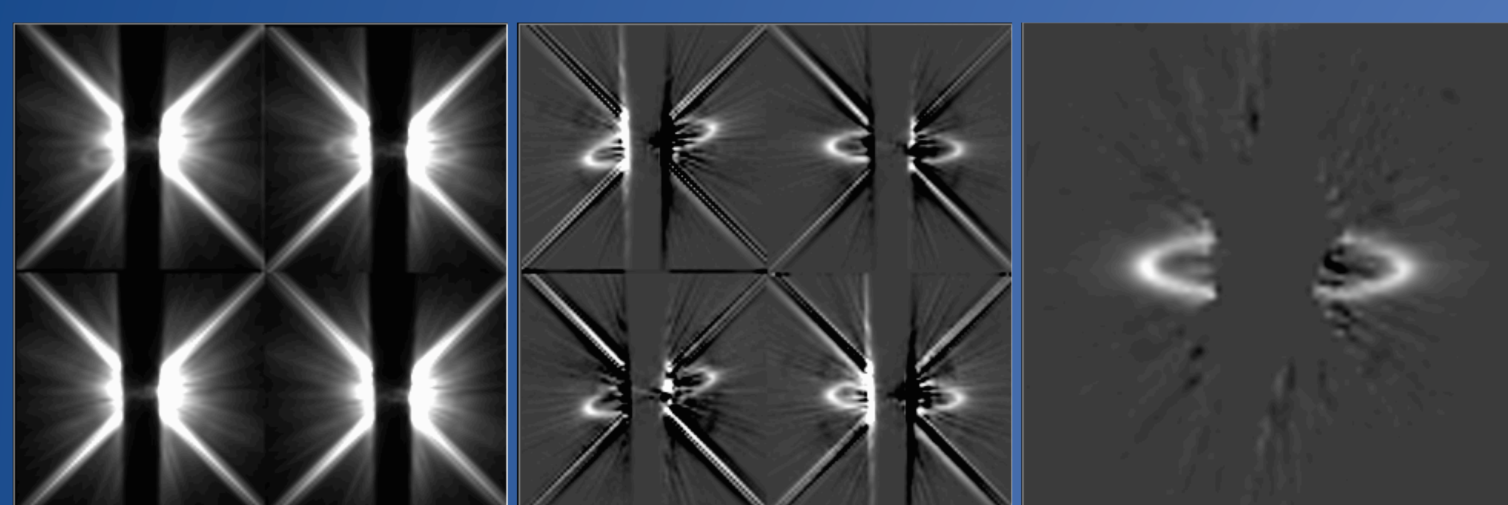

Fig 1a. TOP: The HR 4796A debris ring is visible superimposed upon residual light from the stellar PSF unsuppressed by the STIS coronagraph in two (multiple exposure combined) images with the celestial field reoriented by 16°. BOTTOM: Similarly observed reference star (HR 4748) PSFs.

Fig 1b. By separately subtracting the two HR 4748 PSF templates from the two HR 4796A star+disk images, the circumstellar disk is better revealed. Artifacts from PSF subtraction are largely rotationally invariant, though temporal changes in the PSF result in imperfect and slightly different subtractions.

Fig 1c. Final analysis quality image. The four PSF subtracted images, co-registered on the location of the star are rotated to a common celestial frame and median combined after individually masking the STIS occulting wedge and diffraction spikes from the optical telescope assembly.

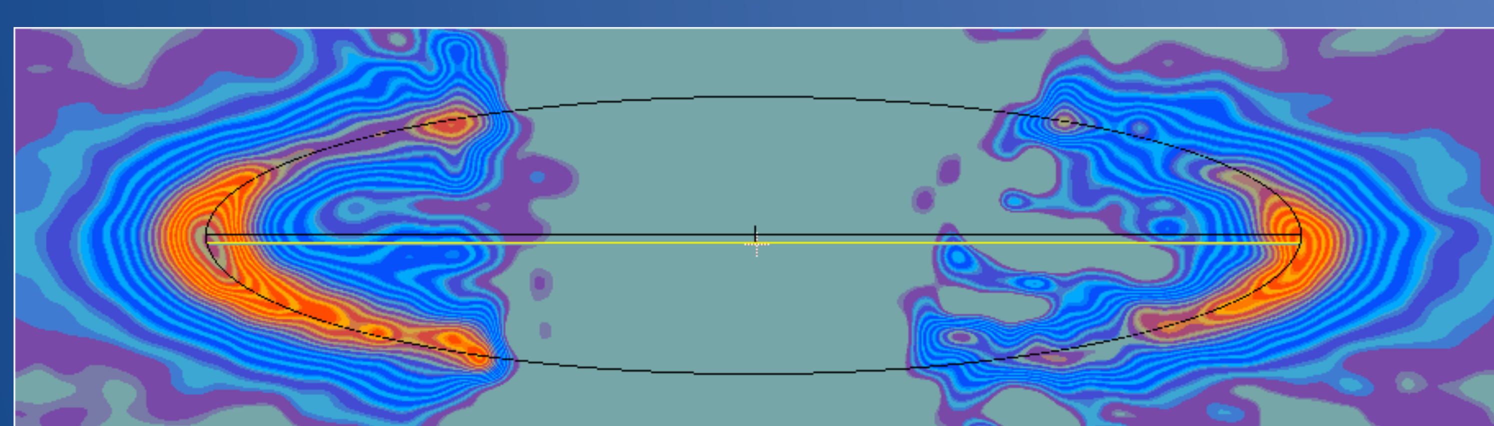

Fig 2. Best-fit radial-peak SB ellipse (black) from isophote fitting of seven SB contours at, and flanking, the radius of the ring ansae. Yellow line connects ansal photocenters – displaced toward the brighter side semi-minor axis due to forward scattering.

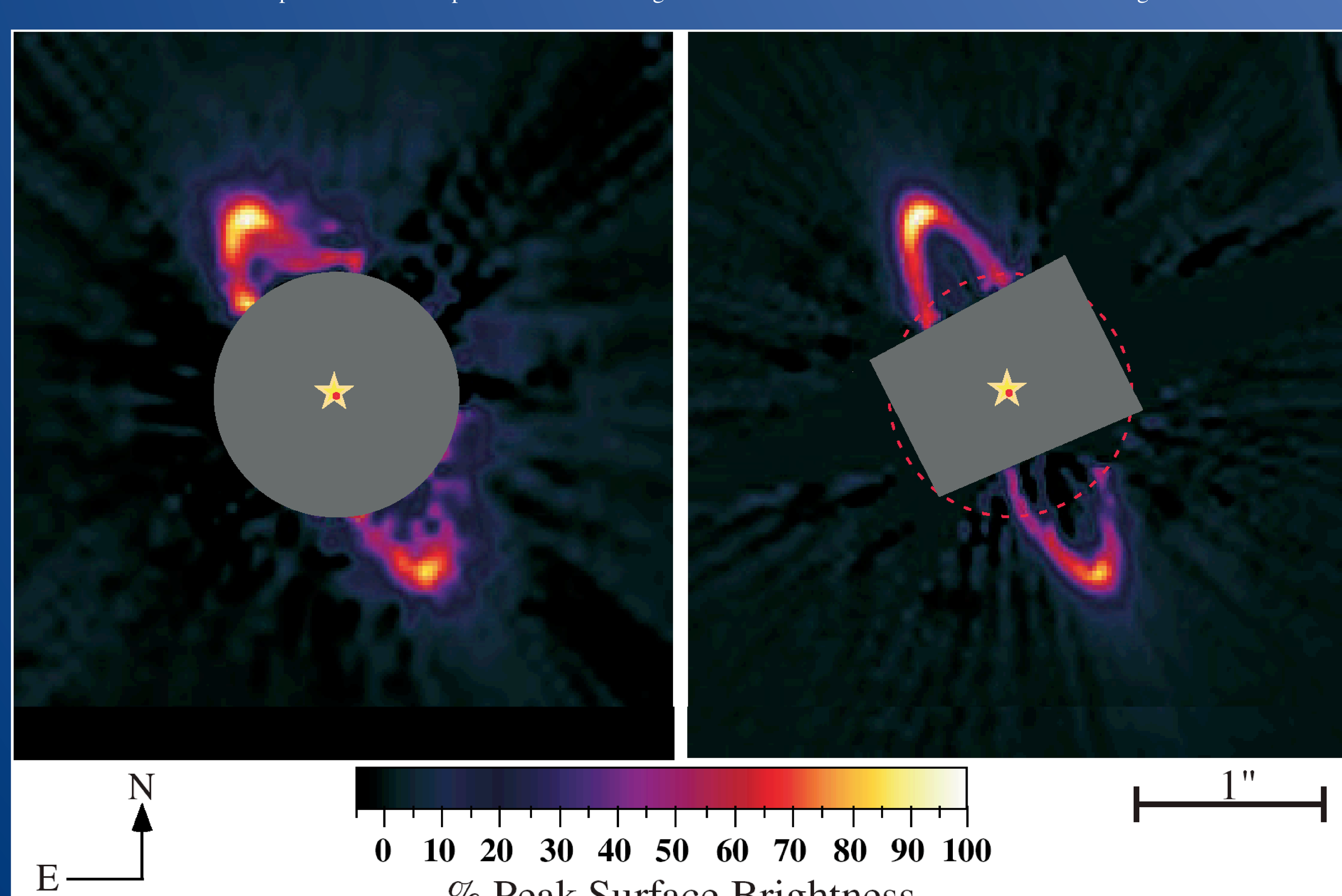

Fig 3. NICMOS 1.1 μm (left) and STIS 0.6 μm (right) images of the HR 4796A circumstellar debris ring. The red dots mark the center of the ring (as determined from the STIS image), offset from the location of the coronagraphically occulted star. Both images show a decrement in ring brightness at celestial PA ≈ 230°.

RING GEOMETRY

We exploit the ~ 70 mas spatial resolution of the STIS optical imaging data to improve upon the initial determination of the geometrical parameters of the HR 4796A circumstellar debris ring derived from the NICMOS scattered light images by Schneider et al. (1999). By ring geometry, with measurement results presented in Table 1, we mean: (a) the location of its center — determined separately from the position of the star, (b) its ellipticity (apparent eccentricity; we interpret the apparent ellipticity as evidence for a disk which is intrinsically circular, or nearly so, and inclined to our line of sight and use it to calculate an inclination), (c) the major axis length that corresponds to the ridge of maximum surface brightness (SB) in a deprojected ellipse, and (d) the major axis celestial position angle of the apparent ellipse.

MEASUREMNT METHODS. (1) We fit ellipses to ring isophotes at the 25%, 50%, 75% (interior and exterior to the peak), and 100% peak SB levels normalized at each azimuth (in 5° deprojected increments) to the maximum SB at each position angle in each azimuthal bin (excluding data behind and immediately adjacent to the coronagraphic wedge and diffraction spikes). All of the geometrical parameters, except the semimajor, axis were determined from the mean of the seven isophotal fits; the semimajor axis length (which corresponds to a deprojected radius of maximum SB) was determined from the 100% isophotal contour alone. (2) We built a model of the disk assuming an elliptical ring with a SB profile across the ring described by a Gaussian. The model geometry is defined by five free parameters, corresponding to those independently measured as described above: ellipse center (x and y), semimajor axis length and orientation, and inclination. The disk model also includes two other free parameters: the ring Gaussian width and overall intensity normalization (i.e., a scale factor to match the total disk flux density). For this purpose, we modeled the forward scattering with a Henyey–Greenstein prescription. We modeled the ansal asymmetry as a smooth sine function peaked along the major axis at the northeast ansa and decreasing to the southwest side with an amplitude equal to the photometrically measured asymmetry. The model free parameters were iteratively adjusted to fit the observational data with χ^2 minimization. The geometrical parameters determined by the two independent methods agree very well. The averages from the two methods (and their resulting uncertainties) are presented in Table 1.

THE WIDTH OF THE RING (and implication for vertical structure)

The STIS image informs that the HR 4796A light-scattering disk grains are radially confined to a narrow zone circumscribing the star: photometrically, 8.7% of the debris ring's 154 AU diameter. Across the brighter (NE) ansa, the photometric FWHM of the ring is 0.197" (14.3 AU), but the brightness fall-off interior to the 76 AU characteristic radius is somewhat steeper than exterior, indicating a sharper inner cut-off than outer truncation (*Fig 5*). Subtracting in quadrature the 0.070" FWHM of the STIS PSF, we find the intrinsic $HWHM_{inner}$ = 0.082" and $HWHM_{outer}$ = 0.102." The FWHM around the ring broadens with increasing azimuth angle from the ansae (toward the brighter-side minor axis of the ring) with a 0.222" azimuthally medianed Gaussian FWHM. This effect is opposite what is expected for a geometrically flat disk, and is indicative of scattering by dust above the disk mid-plane.

CENTRAL CLEARING, OUTER TRUNCATION, AND RING PARTICLE CONFINEMENT

A central "hole" in the HR 4796A light-scattering disk is seen in the Schneider et al. (1999) near-IR images, and a similar central clearing to an instrumentally limited inner radius of ~ 0.5" (35AU) is apparent in the STIS optical image (*Fig 3*). Telesco et al. (2000) found the 11–18 μm mid-IR optical depth in the central zone < 3%, with the disk's emitting regions spatially coincident with the dust-scattered starlight at optical and near-IR wavelengths. Small particles may be cleared from the system by radiation pressure and Poynting–Robertson drag on timescales much shorter than the estimated ~ 8 Myr age of HR 4796A if the dust were not replenished and/or confined. The number of grains in the ring, as inferred from the mid-IR observations, implies that the dust in the ring should be collisionally dominated. It is likely that mutual collisions disintegrate large grains until they are small enough to be removed by radiation pressure. Then, the absence of dust interior to the starlight-scattering ring indicates a corresponding absence of large bodies located there (Kenyon et al. 1999; ApJ 524 L119). The outer "truncation" of the disk might be dynamically aided by the M-star companion to HR 4796A, though it is at a projected (minimum) distance of ~ 500 AU. Dynamical models of the ring must also reproduce the relatively sharp inner, and slightly less steep outer ring boundaries. Such tight bounding might be manifested by the shepherding of the ring particles by co-orbital bodies Goldreich & Tremaine 1979; Nature 277 97), loosely analogous, for example, to structures seen in the Saturnian rings, but here on solar system size scales.

FORWARD SCATTERING BY THE DISK GRAINS

For an inclined disk, the side centered on scattering phase angle (SPA) 0° (line of sight toward the observer) is seen primarily in forward scattered starlight while the other half (centered on SPA 180°) is seen primarily in light that is backscattered. Separately, the HR 4796A disk is clearly brighter on the NE side (SPA 90°) than toward the SW (SPA 270)°. To determine if the ring dust displays significant azimuthally nonisotropic scattering, we measured the total disk flux density in symmetrically placed sectors within the four readily visible quadrants of the disk between 5° and 20° from the and within 0.8° to 1.5° from the star. We characterize asymmetry measurements in terms of a Henyey-Greenstein phase function parameter, g (a metric for "front-to-back" light-scattering asymmetry), at the best-fit inclination of 14.1° from edge on following the formulism of McCabe et al. (2002). The best fit for the measured inter-sector flux density ratios is g = 0.16 ± 0.06; evidence for forward scattering at the 2.7 σ level of confidence. Additionally, the displacement of a line (yellow in *Fig 4*) joining the ansal photocenters from the major axis of the best fit ellipse line (blue in *Fig 4*) is indicative of forward scattering.

ANSAL ASYMMETRY & STELLOCENTRIC OFFSET

Comparing debris ring sectors ± 20° from major axis from both ansae and 0.8" ≤ r < 1.5" from the star in the STIS optical passband, the SW side of the disk appears only only 74% ± 7% as bright as on the NE side (*Fig 4*). Similar brightness asymmetries are seen in the near- (Schneider et al. 2001; ASP Conf. Ser. 241, 203) and mid- (Telesco et al 2000; ApJ 530 329) IR. Wyatt et al (1999) suggested the mid-IR asymmetry could arise from a "pericenter glow"; a forced eccentricity of 6.4% $(R_{sw} - R_{NE})/R_{mean}$ to explain the mid-IR asymmetry caused by the grains on one side of the disk grains being closer to the star (and thus heated to higher temperature) than the other. From the STIS image we measure a stellocentric offset of 19 ± 6 mas, or 1.4 AU (*Fig 6*). This radial offset asymmetry of 3.7% along the major axis would result in only a 14% difference in ansal SB (due to the r^{-2} dilution of the stellar radiation field) for a homogeneous, azimuthally uniform, distribution of disk grains. Given an orbital period of ~ 350 years at the ring radius of 76 AU, and the age of the star of ~ 8 Myr, one would expect a well-mixed, not azimuthally segregated population of grains with different scattering efficiencies. We suggest the possibility of a dynamic redistribution of the grains, through perturbations or resonant interactions with co-orbital bodies, leading to azimuthally confined regions of enhanced particle densities (e.g., as causally described by Kuchner & Holman (2003; ApJ 588 1110).

AN INTRA-RING GAP?

We note the appearance of a correlated decrement in the ring brightness at a position angle (eastward from north) of 230° ± 10° in both the NICMOS and STIS images (*Fig 3*). The statistical significance of this is not strong in the individual images; however, the correlation of this "feature" in the two images, taken at significantly different field orientations, wavelengths (PSF subtraction artifacts spatially scale with wavelength), and instruments, is intriguing and suggests there might be a gap in the distribution of ring particles at that azimuth. This, perhaps, is further evidence (albeit not very strong on its own) of azimuthal sculpting of the grains by gravitational perturbation by one or more undetected bodies of planetary mass. This region is nearly opposite the bright ansa, and is in the direction of HR 4796B, an M-star companion at a P.A. = 225.4° that sits 7.7" away from HR 4796A.

SPECTRAL REFLECTIVITY (COLOR) OF THE DISK GRAINS

We have found the HR 4796A disk grains to be significantly red at optical to the near-IR wavelengths with multi-spectral colors consistent with radiationally evolved tholins (*Fig 7*: Debes et al. 2008; ApJ 673 L191). Intrinsically red grains are also consistent with a collisionally evolved population of particles where the characteristic particle size is larger than the wavelengths of the observations, as opposed to neutral or blue grains which would be more typical of a primordial population of ISM grains. HR 4796A's disk is not the only one to display such red colors. The more substantial disk around HD 100546 also shows red optical scattering (Ardila et al. 2007), as do portions of the similarly thin β Pictoris disk (Golimowski et al. 2006; AJ 131 3109). Perhaps the reddening mechanism (e.g., Andronico et al. 1987; A&A 184 333) is common to both our outer solar system and the cool portions of younger disks around more luminous stars.

For additional information (in press this week; preprint below poster) see:
Schneider, G., Weinberger, A. J., Becklin, E. E., Debes, J. H., & Smith, B. A. 2009, AJ, 137, 53

Table 1 - HR 4796A CIRCUMSTELLAR DEBRIS RING GEOMETRIC PARAMETERS

Position Angle of the Major Axis	27.01° ± 0.16°
Major:Minor Axis Length Ratio	4.10 ± 0.05
Implied Polar Inclination	75.88° ± 0.16°
Ansal Separation (Photocentric Peaks)	41.563 ± 0.088 pixels, 2.107" ± 0.0045"
Major Axis (Best-Fit Ellipse)	41.698 ± 0.108 pixels, 2.114" ± 0.0055"
Henyey-Greenstein *g*	0.16 ± 0.06 (at 0.6 microns)
Ansal SB Asymmetry Factor	0.74 ± 0.07 (at 0.6 microns)

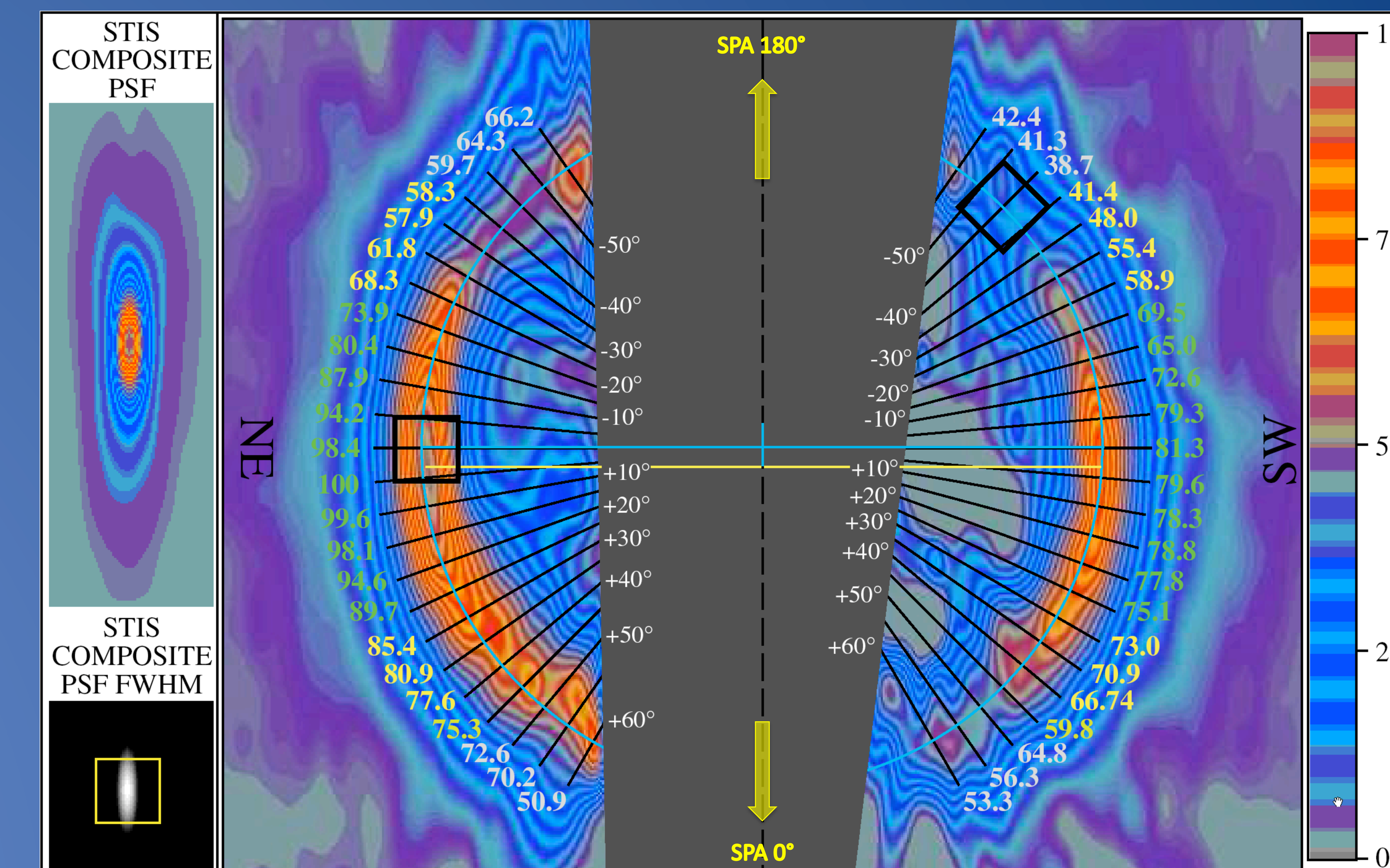

Fig 4. Deprojected image of the disk (with flux conservation) showing SB isophotes. The color bar shows 3.2% intensity isophotes switching from orange to blue at 50% of the peak SB. We fit concentric circles to seven ring isophotes at the 25%, 50%, 75%, and 100% SB levels normalized at each azimuth to the maximum SB at each position angle in each azimuthal bin. Azimuthal samples were made at 5° deprojected increments as marked on the interior of the image. Photometry for these samples was done in apertures fully enclosing the projected FWHM of the STIS PSF, as shown in the bold black squares that were rotated to maintain a fixed inner and outer distance from the ring center. The numbers around the periphery of the disk image give the SB as a percentage of the peak ansal brightness at each fit point along the 100% contour. The light blue circle shows the best fit at the 100% contour. The horizontal blue line shows the ellipse major axis. The yellow line connects the ansae and therefore shows the offset of the ellipse due to forward scattering. Also shown at left are what the STIS PSF looks like when deprojected, (top) on a stretch that shows all of its details, and (bottom) the same PSF clipped at the FWHM to show only the core shape. The yellow square on the lower PSF shows the size of the photometric extraction aperture.

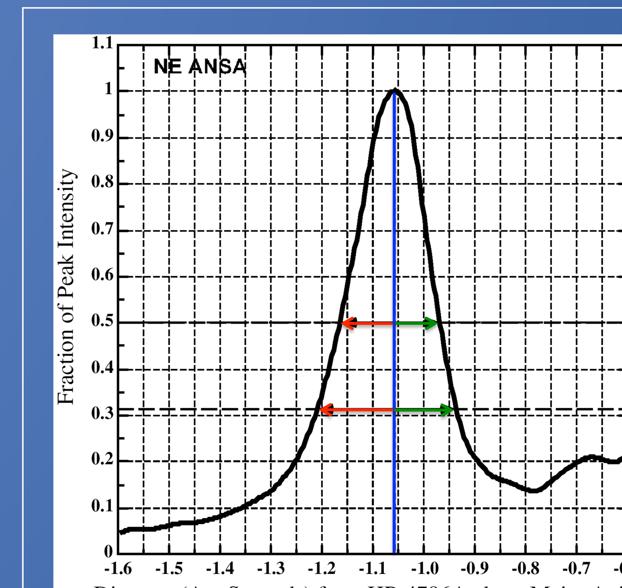

Fig 5. Characteristic width of the HR 4796A ring defined from a cross-sectional profile through the NE ring ansa along the major axis of the best-fit ellipse (BFE). Arrows show the profile's exterior and interior half widths at half-intensity maximum and 1 - 1/e of the maximum. The distance along the major axis is measured from the center of the BFE.

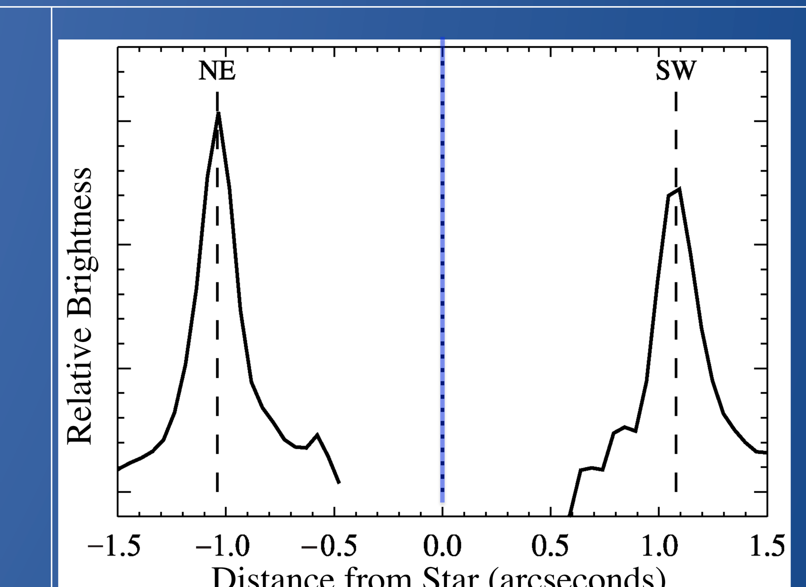

Fig 6. A 50 mas wide slice along the major axis of the disk shows the locations of the NE and SW ansae at respective distances of 1.040" and 1.079" from the star (vertical dashed lines; stellar location at zero is marked with a dotted line). The mid-point between the the ansae, i.e., the ring center, is shifted 19 ± 6 mas away from NE ansa. At the distance to HR 4796 of 72.8 pc, this is a stellocentric offset of 1.4 ± 0.4 AU

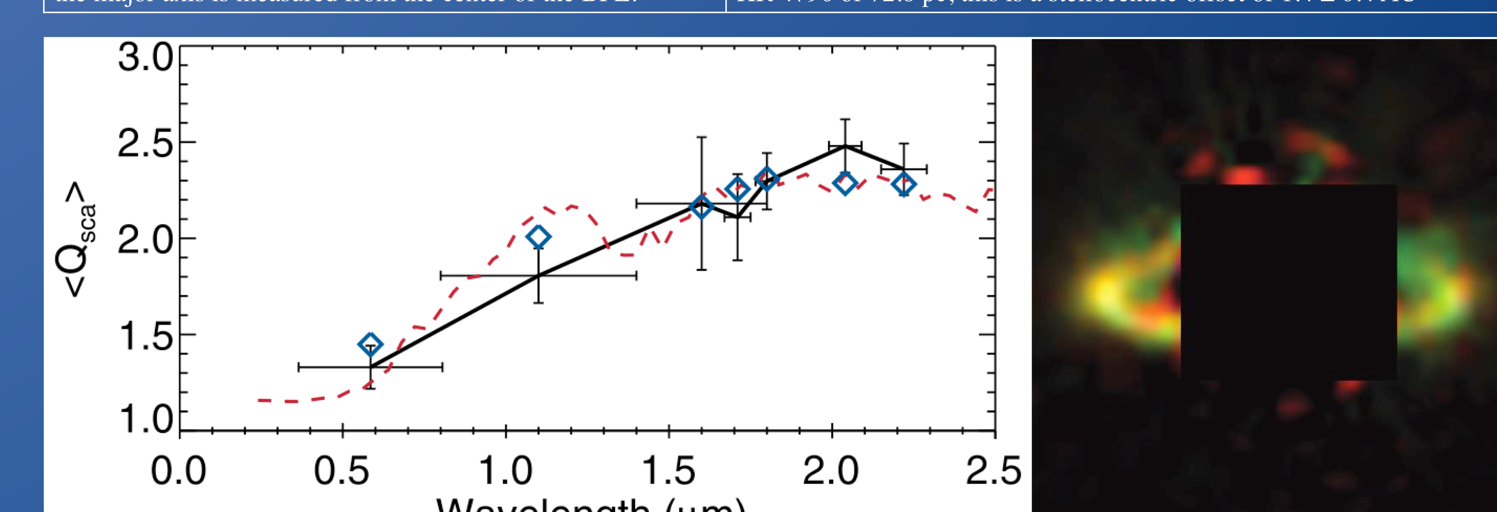

Fig 7. From Debes et al. (2008). Left: An optical/near-IR reflectance spectrum of the HR 4796A debris ring (Q_{sca} is a measure of the wavelength-dependent scattering efficiency of the disk grains) derived from STIS and NICMOS filter-band photometry (from HST GO program 10167) is well-fit by tholins (heteropolymers formed by UV irradiation of organic simple compounds as is seen on small icy bodies in the outer parts of our solar system. Right: False color image of the HR4796A debris ring derived from the STIS 0.6 (blue), NICMOS 1.1 (green) , and NICMOS 1.7 μm images).

This work is based on observations with the NASA/ESA Hubble Space Telescope, obtained at the Space Telescope Science Institute, which is operated by AURA, Inc. under NASA contract NAS2-6555 and supported NASA grants NAG5-3042 and GO 8624 , 10167, and 10177.